ADVANCED MATERIALS
www.advmat.de

# Understanding the Crystal Packing and Organic Thin-Film Transistor Performance in Isomeric Guest–Host Systems

*Anna K. Hailey, Anthony J. Petty II, Jennifer Washbourne, Karl J. Thorley, Sean R. Parkin, John E. Anthony, and Yueh-Lin Loo**

**In order to understand how additives influence the structure and electrical properties of active layers in thin-film devices, a compositionally identical but structurally different guest–host system based on the *syn* and *anti* isomers of triethylsilylethynyl anthradithiophene (TES ADT) is systematically explored. The mobility of organic thin-film transistors (OTFTs) comprising *anti* TES ADT drops with the addition of only 0.01% of the *syn* isomer and is pinned at the mobility of OTFTs having pure *syn* isomer after the addition of only 10% of the isomer. As the *syn* isomer fraction increases, intermolecular repulsion increases, resulting in a decrease in the unit-cell density and concomitant disordering of the charge-transport pathway. This molecular disorder leads to an increase in charge trapping, causing the mobility of OTFTs to drop with increasing *syn*-isomer concentration. Since charge transport is sensitive to even minute fractions of molecular disorder, this work emphasizes the importance of prioritizing structural compatibility when choosing material pairs for guest–host systems.**

Adding fractional amounts of a "guest" material into a "host" matrix is a promising strategy to tune the properties of thin-film active layers in organic electronic devices.[1] For example, such additives have been used as nucleating agents to improve the overall crystallinity in thin films, leading to higher device mobilities in organic thin-film transistors (OTFTs) having such films as active channels.[1,2] However, additives can also have the detrimental effect of suppressing crystallization of the host matrix by disrupting molecular order.[1,3] This undesired consequence is often observed in the distinct case of dopants, which are chosen for their ability to directly tune the electronic properties, rather than for their similarity in chemical structure to the host. Since doping in organic-semiconductor systems is far less efficient than in the inorganic systems from which the technique was borrowed, dopant molar concentrations in excess of 1% are often required to effect the desired electronic changes in the host material.[4] At such high concentrations, the anticipated electronic benefits of doping are often thwarted by insufficient consideration of the structural compatibility of the dopant and host material.[4a,5] Although a wealth of literature exists exploring dopant influence on electronic properties, much less attention has been paid to their influence on structure.[4b,6] Yet, understanding the dopant influence on structure will only become more important as increasingly diverse molecular dopants at higher concentrations are considered. Given how crucial the active-layer microstructure is to overall device performance, we must learn how additives introduce disorder in the host, and how this disorder affects the observed electrical properties in thin-film devices.

Since charges generally travel through intermolecular $\pi$-orbital overlap in molecular semiconductors, the ordering of these molecules is crucial to their ability to transport charge across macroscopic distances.[7] In fact, slight offsets in the $\pi$-orbital overlap between neighboring molecules in thin films can lead to orders-of-magnitude difference in the charge-carrier mobility through the active layer of OTFTs.[8] To minimize additive-induced disorder, several studies have focused on using ultralow additive fractions[3,4] or using molecularly similar guest and host materials, such as pentacene and its fluorinated analogues.[9] However, even guest–host systems comprising molecularly similar materials can produce thin films of such blends with undesirable morphologies. For example, differences in solubility and driving force for crystallization can lead to aggregation that suppresses crystallization.[1] Thus, in this study, we have further stripped unnecessary variables by instead using a "guest" material that is molecularly equivalent to the host material. By using a pair of structural isomers as an analogue for a guest–host system, we can focus on how changes in intermolecular interactions affect electrical performance. Other works have studied the structure and device performance of the extremes in isomeric purity—pure *anti* and/or pure *syn*, often

A. K. Hailey, Prof. Y.-L. Loo
Department of Chemical and Biological Engineering
Princeton University
Princeton, NJ 08544, USA
E-mail: lloo@princeton.edu
A. J. Petty II, J. Washbourne, Dr. K. J. Thorley,
Prof. S. R. Parkin, Prof. J. E. Anthony
Department of Chemistry
University of Kentucky
Lexington, KY 40506, USA
Prof. Y.-L. Loo
Andlinger Center for Energy and the Environment
Princeton University
Princeton, NJ 08544, USA
The ORCID identification number(s) for the author(s) of this article can be found under http://dx.doi.org/10.1002/adma.201700048.

**DOI: 10.1002/adma.201700048**

 

in comparison with the as-synthesized mixture of isomers.[10] Different from works past, this work systematically quantifies the structural changes induced by the progressive addition of an isomer additive across the composition window and explores the electrical property differences that result from such structural disorder.

Our model system is triethylsilylethynyl anthradithiophene (TES ADT), a solution-processable molecular semiconductor. Although ADTs are usually prepared as a mixture of isomers,[11] ADTs can also be prepared as pure *syn* and *anti* isomers due to recent advances in synthesis and purification procedures.[10a–e,12] We use a heavily modified version of these approaches to prepare, for the first time, pure *syn* and *anti* TES ADT. Despite differences in the single-crystal structures of *syn* and *anti* TES ADT, each forms spherulites 1–4 cm in diameter upon solvent-vapor annealing. We have thus used this isomeric guest–host system to determine how the introduction of guest affects the crystal packing and electronic properties, and accordingly, the device performance of OTFTs comprising active layers with increasing guest content.

We first investigated the structure and the electrical behavior of the pure *syn* and *anti* isomers of TES ADT as well as that of the as-synthesized isomer mixture, i.e., "mixed" TES ADT.[13] The absorption spectra of the isomers exhibit subtle differences from which we determined that mixed TES ADT comprises 40% *syn*/60% *anti* (**Figure 1**a). Differential scanning calorimetry (DSC, Figure 1b,c) of mixtures across a range of isomer ratios also reveal systematic differences in thermal transitions from which we confirmed that mixed TES ADT comprises 40% *syn*/60% *anti* isomers. That the melting temperature of *syn* is lower than that of *anti* indicates that the cohesive energy density is lower in *syn* crystals than in those of *anti*. Given that the pairs are isomers and thus chemically equivalent, we correlate the lower cohesive energy density with the presence of increased disorder in *syn* crystals compared to those of *anti*. The melting temperature of TES ADT decreases with increasing *syn* concentration, suggesting that *syn* acts as an impurity in the *anti* matrix, and that smaller crystals are formed at higher *syn* levels. Correspondingly, the crystallization temperature increases with increasing *syn* concentration, indicating that less undercooling is required for these less pure samples to nucleate and solidify. With these observations in mind, and in the context of the guest–host discussions above, we assign *syn* as guest and *anti* as host in our materials system of interest.

We used grazing-incidence X-ray diffraction (GIXD) to obtain the experimental thin-film diffraction patterns of the pure isomers and mixed TES ADT. **Figure 2** compares these thin-film diffraction patterns with those calculated from the corresponding single-crystal structures (Figure S1, Supporting Information). We found that the thin-film and single-crystal structures are comparable for the pure *anti* isomer and mixed TES ADT. The extracted unit-cell dimensions are marginally larger for the thin-film formats compared to their single-crystal counterparts; we believe this difference stems from thermal expansion of the lattices, as thin-film diffraction was conducted at room temperature whereas single-crystal structures were obtained at liquid-nitrogen temperatures. However, the thin-film and single-crystal structures of the pure *syn* isomer are distinct and different. Whereas single crystals of the *syn* isomer

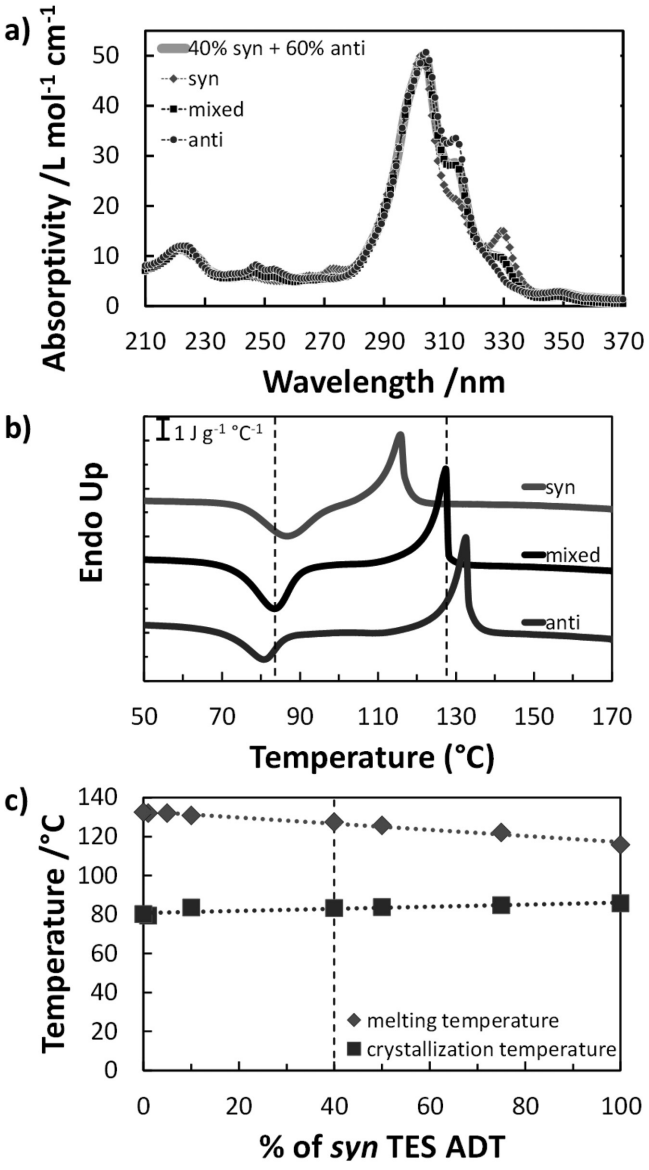


**Figure 1.** a) Solution absorptivity of the *syn* isomer (diamonds), *anti* isomer (circles), and as-synthesized mixture of isomers ("mixed" TES ADT, squares) in pentane. A linear combination of the absorbance spectra of the *syn* and *anti* isomers (gray line) reveals that mixed TES ADT comprises 40/60 *syn* to *anti* isomers. b) Differential scanning calorimetry (DSC) scans of *syn*, mixed, and *anti* TES ADT powders from the third heating cycles. The dashed lines at 83 and 127 °C mark the temperatures at which mixed TES ADT crystallizes and melts, respectively. c) Melting and crystallization temperatures obtained through DSC vary linearly as a function of isomer ratio. The dotted lines represent best fits to the data at known isomer ratios. We used these fits to predict the isomer ratio of mixed TES ADT from its experimental melting and crystallization temperatures (dashed line). The isomer ratio predicted, 40/60 *syn* to *anti* isomers, matches that estimated in (a).

adopt a monoclinic lattice of the *Pc* space group comprising two molecules, thin films of the *syn* isomer instead adopt a triclinic lattice of the $P\overline{1}$ space group comprising a single molecule per analysis with the diffraction pattern calculator (DPC) toolkit.[14] In fact, the thin-film crystal structure of the pure *syn*

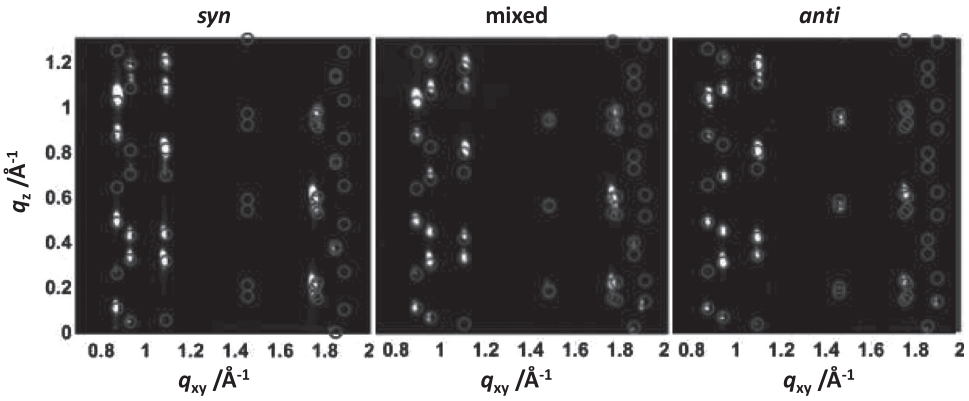


| isomer | SG | *a* [Å] | *b* [Å] | *c* [Å] | *α* [°] | *β* [°] | *γ* [°] | V [Å$^3$] | Z |
|---|---|---|---|---|---|---|---|---|---|
| single crystal | | | | | | | | | |
| ***anti*** | *P*-1 | 6.6825 | 7.2546 | 16.6845 | 97.8261 | 94.7607 | 103.7577 | 773 | 1 |
| **mixed** | *P*-1 | 6.7318 | 7.2511 | 16.6950 | 98.1442 | 94.5289 | 103.9183 | 778 | 1 |
| ***syn*** | *Pc* | 6.3015 | 17.8388 | 13.7739 | 90 | 91.8030 | 90 | 1548 | 2 |
| thin film | | | | | | | | | |
| ***anti*** | *P*-1 | 6.8823 | 7.4069 | 16.6403 | 96.0987 | 92.3087 | 106.2106 | 808 | 1 |
| **mixed** | *P*-1 | 6.9082 | 7.4001 | 16.8674 | 96.343 | 92.2333 | 106.7097 | 819 | 1 |
| ***syn*** | *P*-1 | 6.9387 | 7.3962 | 16.7918 | 96.5714 | 91.2265 | 106.0473 | 821 | 1 |

**Figure 2.** Grazing-incidence X-ray diffraction (GIXD) patterns of thin films comprising the *syn* isomer, the as-synthesized isomer mixture, and the *anti* isomer of triethylsilylethynyl anthradithiophene (TES ADT). The table lists the space group (SG), unit-cell lattice parameters (*a*, *b*, *c*, *α*, *β*, *γ*), unit-cell volume (*V*), and the number of molecules within the unit cell (*Z*) for each in their single-crystal and thin-film formats. The circles overlaying the experimentally obtained GIXD patterns at the top of the figure represent the calculated reflections from DPC toolkit[14] analysis of these GIXD patterns.

isomer appears to be quite similar to the thin-film crystal structures of the *anti* isomer and mixed TES ADT, with differences in the unit-cell lengths and angles of all three structures within 0.3 Å and 1.1°, respectively. Although DPC toolkit only calculates the lattice parameters and not the molecular packing, we assume that the molecular packing of the *syn* isomer in thin films is similar to those of the *anti* isomer and mixed TES ADT given their chemical equivalence and similarities in lattices. It follows that the *anti* crystal structure, i.e., the host, is able to accommodate the introduction of *syn* guest without dramatic molecular reorganization. This assertion is—to first order—true at the macroscale; thin films spanning a range of isomer ratios all exhibit the same spherulitic morphology, as evidenced by the optical images in Figure S2 (Supporting Information). Though second-order effects must also be at play since we do observe smaller spherulites at higher *syn* impurity levels, the similarity of the thin-film *syn*-isomer polymorph to the mixed and *anti* crystal structures has allowed us to extend correlations, drawn between the structure and electrical properties observed in mixed and *anti* OTFTs and the structure and electronic properties calculated from mixed and *anti* single-crystal analysis, to the analysis of *syn* OTFTs as well.

In order to probe the nature of molecular disorder in our isomeric guest–host systems, we turned to computational analysis of the single-crystal structures of mixed and *anti* TES ADT (detailed in the Supporting Information). Since we access a polymorph of *syn* TES ADT instead of its bulk crystal structure in thin films, its single-crystal structure is not relevant for this comparison. While previous work has characterized disorder by comparing the different symmetry point groups of variously arranged molecular pairs (termed "disordermers"),[15] the identical composition of the TES ADT isomers has allowed us to take a simplified approach. Assuming a random spatial distribution of "disordermers," and considering the experimentally observed sulfur occupancies from single-crystal X-ray diffraction, we quantified molecular disorder by comparing the atomic contacts between neighboring anthradithiophene cores. If every *anti* TES ADT molecule adopted the same configuration within a crystal (**Figure 3**), there would be only hydrogen–hydrogen (H–H) contacts between molecules. We thus consider hydrogen–sulfur (H–S) and sulfur–sulfur (S–S) contacts a form of molecular disorder. Consistent with our observations from DSC, we found that the mixed-isomer crystal is more molecularly disordered than the *anti* crystal: H–S and S–S contacts comprise 51% of all contacts in mixed crystals, but only 19% in *anti* crystals (Table S1, Supporting Information). This molecular disorder causes more repulsive interactions between neighboring molecules (Figures S3 and S4, Supporting Information). This intermolecular repulsion is also the likely cause for the larger unit-cell volume adopted by the mixed-isomer crystal than the pure *anti*-isomer crystal.

The presence of additional H–S and S–S contacts in mixed TES ADT results in differences in intermolecular electronic coupling between mixed and *anti* TES ADT single crystals. Both mixed and *anti* TES ADT adopt a 2D brickwork-packing motif, in which significant intermolecular electronic coupling is found along the two *π*-stacking directions ($\pi_1$ and $\pi_2$, see Table S1 in the Supporting Information). The strongest intermolecular electronic coupling in either crystal structure is found along the $\pi_1$-stacking direction in the mixed crystal,

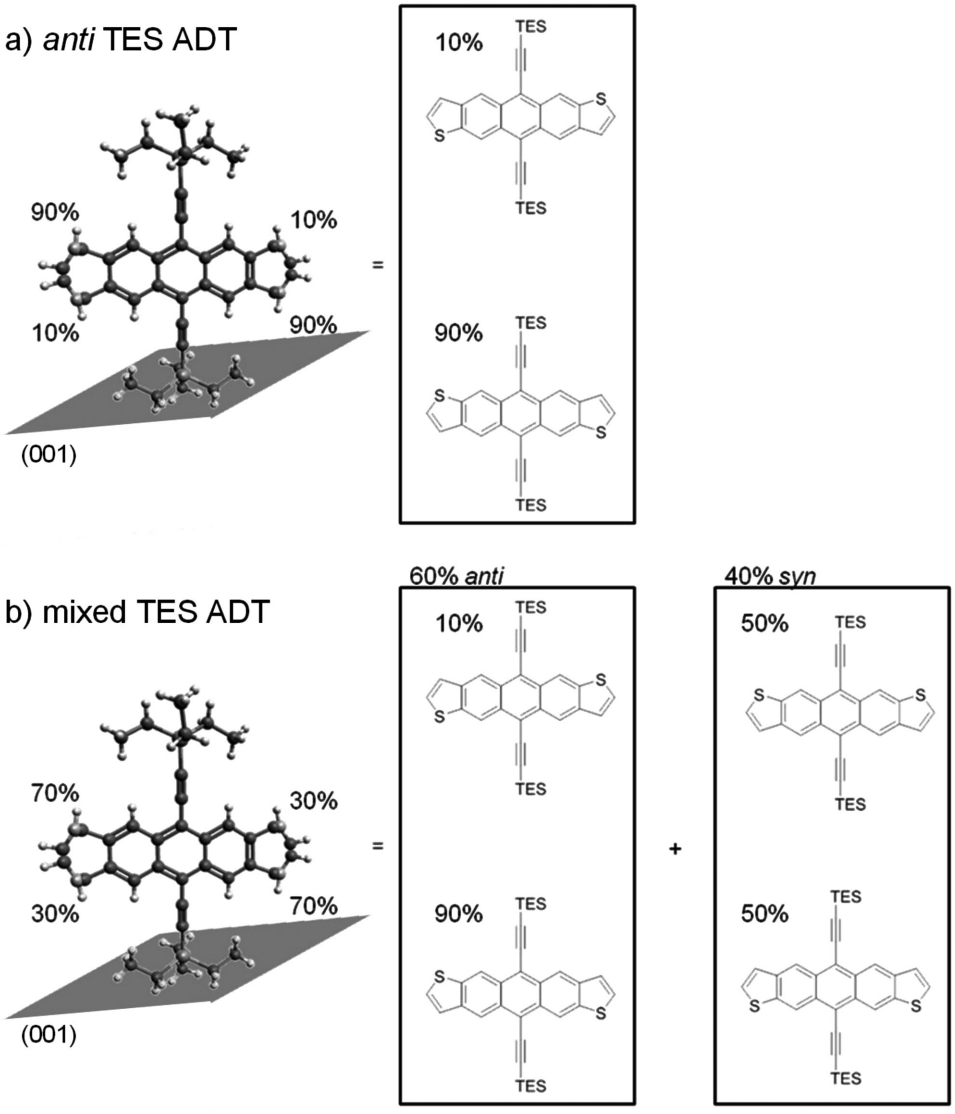


**Figure 3.** Molecular conformations in single crystals of a) the *anti* isomer and b) the as-synthesized isomer mixture. The percentages represent the probability of TES ADT adopting the corresponding configurations with respect to the (001) plane of the unit cell.

which would initially suggest that we should observe higher mobilities in devices comprised of mixed TES ADT compared to those comprised of *anti*. However, the electronic coupling varies more between molecules adopting different relative configurations along a given $\pi$-stacking direction, and varies more overall between the $\pi_1$- and $\pi_2$-stacking directions in the mixed crystal than in *anti*. Due to increased molecular disorder, and the resulting increase in variations in intermolecular electronic coupling, the local trap density should be much higher in the mixed crystal than in *anti*.[10c,15] Since both the trap density and electronic coupling have strong impacts on charge transport, we turned to OTFT measurements to determine the relative impacts of these contributions on device performance.

We investigated the electrical performance of the pure isomers by fabricating OTFTs on pure *syn* and *anti* thin films. The active channels of the transistors ($L$ = 50 µm, $W$ = 204 µm) were made to fit within individual spherulites so interspherulite boundaries, which we have previously shown to act as bottlenecks to charge transport, do not convolute our analysis.[16] Given the distribution of molecular orientation around the radial axis of TES ADT spherulites; however, the active channels necessarily comprise low-angle intraspherulite boundaries.[17] The shallow traps generated by these intraspherulite boundaries, as well as the fact that the intermolecular electronic coupling is pronounced in 2D, are likely responsible for the orientation-independent mobilities observed in devices measured within spherulites of mixed TES ADT[17] and the pure *syn* and *anti* isomers (see Figures S5 and S6 in the Supporting Information). We found that devices within pure *anti* spherulites exhibit a mobility of 1.1 ± 0.2 $cm^2\ V^{-1}\ s^{-1}$. In contrast, devices within pure *syn* spherulites exhibit a twofold lower mobility of 0.6 ± 0.1 $cm^2\ V^{-1}\ s^{-1}$. These results are consistent with our observations from DSC and single-crystal analysis, which indicated that the *syn* isomer is more disordered and behaves effectively as an

impurity to the *anti* isomer. That we observe higher mobilities in *anti* devices than in those of mixed TES ADT suggests that the trap density, stemming from heterogeneities in the configuration of neighboring molecules as detailed above, dominates intermolecular charge transport in TES ADT crystals.

Prior works studying ADT isomers have also observed superior performance in pure *anti* ADT devices compared to those of the pure *syn* isomer.[10b,c] In fact, reports studying the ADT core or asymmetric ADT molecules have found at least an order of magnitude difference between the mobilities of *anti* and *syn* devices.[10c,e] The much smaller difference we find between the mobilities of devices comprising the two TES ADT isomers suggests that the symmetric solubilizing groups reduce the impact of isomeric differences on device performance,[18] consistent with the results of Hallani et al.[10b] The mobility we observe for mixed TES ADT devices is comparable to those of pure *syn* devices. This result is also consistent with prior works, which have found OTFTs comprising *syn* and mixed ADT active layers to exhibit comparable mobilities.[10a,b] These observations indicate that the presence of the *syn* isomer as guest dictates the performance of the *anti* isomer as host, and that the level of disorder is the limiting factor in their device performance. We quantified the amount of guest with which it is necessary to induce such performance-limiting disorder with our investigation across the entire isomeric composition range.

We fabricated OTFTs with active areas comprising different ratios of the *syn* and *anti* isomers. **Figure 4**a shows the resulting mobilities as a function of *syn*-isomer concentration. Since pure *syn* and mixed TES ADT devices exhibit similar mobilities, and since mixed TES ADT comprises 40% *syn*, we expected the high mobility of devices comprising the *anti* isomer to drop to that same level upon the addition of at least 40% *syn*. In fact, we observed that the mobility of the *anti* isomer devices begins to drop after the addition of only 0.01% *syn* and plummets to that of the *syn* isomer devices after the addition of only 10% *syn*. A first observation that the guest influence on the host electronic properties is not additive, our study identifies the defect-sensitive range and plateau point of our *anti*-isomer host material's electronic properties. As we have shown, a small amount of additive, even one that is compositionally identical and as structurally similar to the host material as TES ADT isomers, can have a dramatic effect on the host material's electronic properties.

In order to probe this trend, we calculated the subthreshold swing (SS) for each device as a proxy to the density of shallow traps. Figure 4b shows that the SS increases as the mobility decreases with increasing concentration of *syn* TES ADT. Consistent with our single-crystal analysis, this result suggests that the introduction of *syn* TES ADT increases the shallow-trap density through the introduction of local disorder. After the addition of only 10% *syn*, charge transport appears dominated by the additional shallow traps induced by the *syn* impurity. We thus observe that even a small amount of additive can disorder the host material enough to induce a significant density of additional shallow traps in the active layer. As previously mentioned, some prior works attributed the similar mobilities observed between *syn* and mixed-isomer devices to similar extents of molecular disorder between syn and mixed-isomer active layers.[10a,b] However, neither of these works were able to correlate this disorder with the density of shallow traps. In fact, Hallani et al. speculated that the effect of charge trapping due to disorder on the device mobility was minimal, as the subthreshold swings observed in devices were small.[10b] Although the SS observed in our devices are similarly small, by methodically varying the *syn*-guest concentrations, we clearly observe that the shallow-trap density tracks with the extent of disorder in the *anti*-host matrix. The twofold mobility decrease upon the introduction of this disorder suggests that the mobility may be more sensitive to small changes in the shallow-trap density than previously thought.

To examine how the film structure changes with the incorporation of *syn*, we analyzed the GIXD patterns of thin films

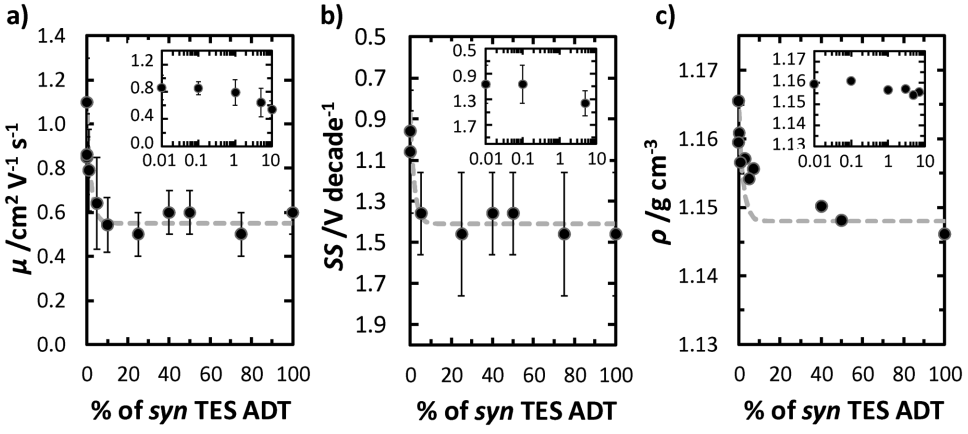


**Figure 4.** a) Mobility ($\mu$), b) subthreshold swing (SS), and c) unit-cell density ($\rho$) as a function of *syn*-isomer concentration. For films comprising both isomers, the measurement error on the percentage of *syn* TES ADT is 10%–20% of its order of magnitude; e.g., "75% *syn*" is (75 ± 2)%, and "0.01% *syn*" is (0.01 ± 0.002)%. The device measurements at each isomer ratio represent the average results of at least 14 devices tested over two different films. In each panel, the data are fitted (dashed line) with an empirical equation of $f(x) = c \exp(-50x) + f_0$, where $c$ accounts for the scale of the data, the coefficient of 50 controls the sharpness of the curve downward, and $f_0$ represents the average value to which $f(x)$ plateaus. That each data set can be described with the same functional form indicates the same relationship with *syn*-isomer concentration for all three parameters. The *y*-axis in (b) is plotted in reverse to highlight the same trend across all the three data sets. The insets in (a)–(c) highlight data in the 0.01%–10% *syn* range, with the *x*-axis shown in log scale.

comprising different *syn*- and *anti*-isomer ratios. We used the DPC toolkit program[14] to determine how and by how much the unit-cell lattice parameters vary with the *syn*-guest concentration. Just as we observed in single crystals, the unit cell of thin-film mixed TES ADT is less dense than that of a*nti* TES ADT. We found that the unit-cell density decreases with increasing *syn* concentration (Figure 4c), and that this trend correlates with both the decrease in OTFT mobility and increase in SS. We tracked the change in individual unit-cell lattice-parameter dimensions with the isomer ratio in Figure S7 (Supporting Information). The expansion of the unit cell generally corresponds to a lengthening of the *c*-axis and the equivalent of shearing the unit cell, yielding a smaller $\beta$ angle. The anisotropic adjustment of the unit-cell lattice suggests that the molecules are rearranging themselves—albeit subtly—within the unit cell. Thus, consistent with single-crystal analysis, the *anti* unit cell must deform in order to accommodate *syn* isomers, and this accommodation simultaneously induces shallow traps that restrict the mobilities observed in OTFTs. Prior works have simply noted that isomeric purity has little impact on solid-state packing.[10a–c,f–i] In stark contrast, our structural study that directly tracks the deformation of the host lattice upon the introduction of disorder as a function of *syn*-guest concentration has proven otherwise. The observation of this deformation reinforces the idea that subtle changes in the unit-cell dimensions can belie significant changes in intermolecular interactions.[8]

Our computational analysis of mixed and *anti* TES ADT single crystals thus correlates well with the trends we observe in the structure and electrical properties across the range of *syn*-guest concentrations in thin films. From the moment the *syn* concentration in the film is increased, the molecular disorder, defined by the percentage of H–S and S–S contacts, is increased. This disorder enhances repulsion between molecules, causing the molecules to adopt a more expanded lattice compared to that of *anti* TES ADT. We observe this expansion as an increase in unit-cell volume with increasing *syn* concentration. Furthermore, Figure S4 (Supporting Information) suggests that the strength of intermolecular repulsion eventually tapers off, which could explain the plateau in unit-cell density at higher *syn* concentrations. The more disordered lattice increases the local trap density,[10c,15] which we observe as a higher SS in devices with higher *syn* content. Interestingly, this overwhelming density of traps pins the mobility at pure *syn* TES ADT device levels after the addition of only 10% *syn*. Thus, by methodically varying the *syn*-guest concentration, we are able to both deduce the nature of guest-induced disorder and precisely quantify the defect-sensitive range and plateau point of our *anti*-isomer host material's structure and electronic properties, which cannot be easily accomplished by examining the characteristics of the pure and mixed isomers alone.

In this study, we used a guest–host system based on closely related structural isomers to study the effect of additive concentration on crystal packing and transistor performance. This guest–host system allowed us to probe the effect of a subtle form of molecular disorder on the electrical properties observed in devices. We found that the mobility decreased upon addition of the smallest amounts of *syn* isomer and dropped by a factor of two after only 10% *syn* was added. Performance remained pinned at the lower mobility of the *syn* device at higher *syn* concentrations. This decrease in mobility with increasing *syn* concentration corresponds to a simultaneous increase in the shallow-trap density and a decrease in the unit-cell density. We determined that the unit-cell density decreases with increasing *syn* concentration due to increasing repulsion between molecules. These more repulsive interactions also signal more disorder in the charge transport pathway, increasing charge trapping and thus decreasing mobilities in organic thin-film transistors comprising more of the *syn* isomer.

These results suggest that device performance is sensitive to the amount of molecular disorder, even at minute fractions. Our work thus highlights the importance of understanding and prioritizing structural compatibility when choosing material pairs for guest–host systems. Since the predicted electronic properties of the guest or host material may not be accessible due to morphological constraints in blended films, the blended thin-film structure may be the most important parameter to optimize when designing guest–host systems for organic electronic device applications.

## Experimental Section

*Isomer-Pure TES ADT Synthesis*: Details of synthesis procedures are provided in the Supporting Information.

*Film Formation*: Substrates comprising 300 nm thick thermally grown $SiO_2$ on highly doped-Si wafers (process specialties) were consecutively sonicated in acetone, isopropyl alcohol, and deionized water and then dried with house nitrogen. Pure-isomer solutions were prepared by dissolving *anti* and *syn* TES ADT in toluene separately. Solutions comprising various *syn*-isomer fractions were prepared by mixing the pure-*anti* solution with an aliquot of a diluted pure-*syn* solution. Final solution concentrations were fixed at 2 wt% to maintain a 100 nm film thickness. The solutions were then spin-coated onto the precleaned substrates at 1000 RPM for 60 s. The substrates were subsequently annealed at 90 °C for 2 min on a hot plate to remove residual solvent from the film. To induce macroscopic crystallization of TES ADT thin films, a solvent-vapor annealing chamber (described in Lee et al.[19]) was used to expose the samples to 0.016 vol% 1,2-dichloroethane vapor in a $N_2$ carrier gas.

*Transistor Fabrication and Measurements*: Top-contact electrodes were deposited onto TES ADT thin films by thermally evaporating 100 nm thick gold through a shadow mask. Measurements were conducted in a Lakeshore probe station under ambient conditions in the saturation regime using an Agilent 4145B semiconductor parameter analyzer. Contact resistance thus does not play a role in our analysis. The capacitance of the 300 nm thick $SiO_2$ dielectric layer was 11.7 nF $cm^{-2}$. The channel length and width were 50 and 204 µm, respectively.

*Grazing-Incidence X-Ray Diffraction*: GIXD was performed at the G2 station at the Cornell High Energy Synchrotron Source. X-rays at 11.3 keV were selected using a beryllium single-crystal monochromator. A $0.2 \times 3$ (V × H) $mm^2$ beam was defined with motorized slits. The X-ray beam was aligned between the critical angles of the film and substrate, at 0.16° with respect to the substrate. Scattered intensity was collected using a 640-element 1D diode array. All GIXD images have been background subtracted. TES ADT films used for GIXD experiments were deposited and crystallized in the same manner as described above.

*UV–vis Absorption*: Absorption spectra were collected on an Agilent 8453 spectrometer using quartz spectrophotometer cells with a 1 cm path length. Solutions were prepared in pentane with concentrations between 0.003 and 0.09 M.

*Differential Scanning Calorimetry*: DSC scans were collected using a TA Instruments Q2000 DSC with aluminum sample and reference pans. The baseline from the reference scan was automatically subtracted from

the sample scan. Each sample comprised ≈2 mg of crystalline powder. The temperature was scanned between 50 and 170 °C at a rate of 2 °C $min^{-1}$ for three heating and cooling cycles.

*Single Crystal X-Ray Diffraction*: Diffraction data were collected on either a Nonius Kappa charge-coupled device (CCD) or a Bruker-Nonius X8 Proteum diffractometer. The data sets were refined and the structures solved as described in the CIFs.

*Electronic Coupling Calculations*: Calculations were performed with Gaussian09,[20] using the B3LYP functional[21] with the 6-31G(d) basis set.[22] The localized monomer orbital approach[23] was used to account for any site energy differences between interacting molecules. The major molecular alignments observed in the crystal structures were considered.

*Pairwise Interaction Energy Decomposition Analysis (PIEDA)*: PIEDA[24] was performed with GAMESS-US software[25] at the MP2 level using the cc-pVDZ basis set.[26] Atomic coordinates for all input files were taken directly from the crystal structures, including the disordered atoms.

[CCDC 152574 and 1525475 contain the supplementary crystallographic data for this paper. These data can be obtained free of charge from The Cambridge Crystallographic Data Centre via www.ccdc.cam.ac.uk/data_request/cif.]

## Supporting Information

Supporting Information is available from the Wiley Online Library or from the author.

## Acknowledgements

Y.-L.L. acknowledges the National Science Foundation (NSF) MRSEC program through the Princeton Center for Complex Materials (DMR-1420541) and the Designing Materials to Revolutionize and Engineer our Future (DMREF) program through DMR-1627453. J.E.A. acknowledges the DMREF program through DMR-1627428. Part of this research was conducted at the Cornell High Energy Synchrotron Source, which was supported by the NSF and the National Institutes of Health/National Institute of General Medical Sciences (DMR-1332208). A.K.H. was supported by a NSF Graduate Research Fellowship.

## Keywords

disorder, guest–host systems, isomers, organic semiconductors, organic thin-film transistors

Received: January 4, 2017
Revised: February 23, 2017
Published online: April 12, 2017

[1] S. S. Lee, S. Muralidharan, A. R. Woll, M. A. Loth, Z. Li, J. E. Anthony, M. Haataja, Y.-L. Loo, *Chem. Mater.* **2012**, *24*, 2920.
[2] a) Z. Wei, H. Xi, H. Dong, L. Wang, W. Xu, W. Hu, D. Zhu, *J. Mater. Chem.* **2010**, *20*, 1203; b) L. Ma, W. H. Lee, Y. D. Park, J. S. Kim, H. S. Lee, K. Cho, *Appl. Phys. Lett.* **2008**, *92*, 063310; c) S. S. Lee, C. S. Kim, E. D. Gomez, B. Purushothaman, M. F. Toney, C. Wang, A. Hexemer, J. E. Anthony, Y.-L. Loo, *Adv. Mater.* **2009**, *21*, 3605.
[3] A. Higgins, S. K. Mohapatra, S. Barlow, S. R. Marder, A. Kahn, *Appl. Phys. Lett.* **2015**, *106*, 163301.
[4] a) X. Lin, G. E. Purdum, Y. Zhang, S. Barlow, S. R. Marder, Y.-L. Loo, A. Kahn, *Chem. Mater.* **2016**, *28*, 2677; b) I. Salzmann, G. Heimel, M. Oehzelt, S. Winkler, N. Koch, *Acc. Chem. Res.* **2016**, *49*, 370.
[5] S. Olthof, W. Tress, R. Meerheim, B. Lüssem, K. Leo, *J. Appl. Phys.* **2009**, *106*, 103711.
[6] B. Lüssem, M. Riede, K. Leo, *Phys. Status Solidi A* **2013**, *210*, 9.
[7] M. Mas-Torrent, C. Rovira, *Chem. Rev.* **2011**, *111*, 4833.
[8] G. Giri, E. Verploegen, S. C. Mannsfeld, S. Atahan-Evrenk, H. Kim do, S. Y. Lee, H. A. Becerril, A. Aspuru-Guzik, M. F. Toney, Z. Bao, *Nature* **2011**, *480*, 504.
[9] J. B. Sherman, K. Moncino, T. Baruah, G. Wu, S. R. Parkin, B. Purushothaman, R. Zope, J. Anthony, M. L. Chabinyc, *J. Phys. Chem. C* **2015**, *119*, 20823.
[10] a) D. Lehnherr, A. R. Waterloo, K. P. Goetz, M. M. Payne, F. Hampel, J. E. Anthony, O. D. Jurchescu, R. R. Tykwinski, *Org. Lett.* **2012**, *14*, 3660; b) R. K. Hallani, K. J. Thorley, Y. Mei, S. R. Parkin, O. D. Jurchescu, J. E. Anthony, *Adv. Funct. Mater.* **2015**, *26*, 2341; c) M. Mamada, H. Katagiri, M. Mizukami, K. Honda, T. Minamiki, R. Teraoka, T. Uemura, S. Tokito, *ACS Appl. Mater. Interfaces* **2013**, *5*, 9670; d) M. Nakano, K. Niimi, E. Miyazaki, I. Osaka, K. Takimiya, *J. Org. Chem.* **2012**, *77*, 8099; e) R. K. Hallani, K. J. Thorley, A. K. Hailey, S. R. Parkin, Y.-L. Loo, J. E. Anthony, *J. Mater. Chem. C* **2015**, *3*, 8956; f) B. Wex, B. R. Kaafarani, R. Schroeder, L. A. Majewski, P. Burckel, M. Grell, D. C. Neckers, *J. Mater. Chem.* **2006**, *16*, 1121; g) J. L. Brusso, O. D. Hirst, A. Dadvand, S. Ganesan, F. Cicoira, C. M. Robertson, R. T. Oakley, F. Rosei, D. F. Perepichka, *Chem. Mater.* **2008**, *20*, 2484; h) X. Liu, M. A. Burgers, B. B. Y. Hsu, J. E. Coughlin, L. A. Perez, A. J. Heeger, G. C. Bazan, *RSC Adv.* **2015**, *5*, 89144; i) S. Shinamura, I. Osaka, E. Miyazaki, A. Nakao, M. Yamagishi, J. Takeya, K. Takimiya, *J. Am. Chem. Soc.* **2011**, *133*, 5024; j) Z. Bao, B. Wex, B. R. Kaafarani, R. Schroeder, L. A. Majewski, M. Grell, D. C. Neckers, D. J. Gundlach, *Proc. SPIE* **2005**, *5940*, 594004; k) S. L. Suraru, C. Burschka, F. Wurthner, *J. Org. Chem.* **2014**, *79*, 128; l) J.-S. Wu, C.-T. Lin, C.-L. Wang, Y.-J. Cheng, C.-S. Hsu, *Chem. Mater.* **2012**, *24*, 2391.
[11] J. G. Laquindanum, H. E. Katz, A. J. Lovinger, *J. Am. Chem. Soc.* **1998**, *120*, 674.
[12] B. Tylleman, C. M. L. Vande Velde, J.-Y. Balandier, S. Stas, S. Sergeyev, Y. H. Geerts, *Org. Lett.* **2011**, *13*, 5208.
[13] M. M. Payne, S. A. Odom, S. R. Parkin, J. E. Anthony, *Org. Lett.* **2004**, *6*, 3325.
[14] A. K. Hailey, A. M. Hiszpanski, D. M. Smilgies, Y.-L. Loo, *J. Appl. Crystallogr.* **2014**, *47*, 2090.
[15] K. J. Thorley, C. Risko, *J. Mater. Chem. C* **2016**, *4*, 4040.
[16] A. K. Hailey, S.-Y. Wang, Y. Chen, M. M. Payne, J. E. Anthony, V. Podzorov, Y.-L. Loo, *Adv. Funct. Mater.* **2015**, *25*, 5662.
[17] S. S. Lee, M. A. Loth, J. E. Anthony, Y.-L. Loo, *J. Am. Chem. Soc.* **2012**, *134*, 5436.
[18] Y. Jiang, J. Mei, A. L. Ayzner, M. F. Toney, Z. Bao, *Chem. Commun.* **2012**, *48*, 7286.
[19] S. S. Lee, S. B. Tang, D. M. Smilgies, A. R. Woll, M. A. Loth, J. M. Mativetsky, J. E. Anthony, Y.-L. Loo, *Adv. Mater.* **2012**, *24*, 2692.
[20] M. J. Frisch, G. W. Trucks, H. B. Schlegel, G. E. Scuseria, M. A. Robb, J. R. Cheeseman, G. Scalmani, V. Barone, B. Mennucci, G. A. Petersson, H. Nakatsuji, M. Caricato, X. Li, H. P. Hratchian, A. F. Izmaylov, J. Bloino, G. Zheng, J. L. Sonnenberg, M. Hada, M. Ehara, K. Toyota, R. Fukuda, J. Hasegawa, M. Ishida, T. Nakajima, Y. Honda, O. Kitao, H. Nakai, T. Vreven, J. A. Montgomery Jr., J. E. Peralta, F. Ogliaro, M. J. Bearpark, J. Heyd, E. N. Brothers, K. N. Kudin, V. N. Staroverov, R. Kobayashi, J. Normand, K. Raghavachari, A. P. Rendell, J. C. Burant, S. S. Iyengar, J. Tomasi, M. Cossi, N. Rega, N. J. Millam, M. Klene, J. E. Knox, J. B. Cross, V. Bakken, C. Adamo, J. Jaramillo, R. Gomperts, R. E. Stratmann, O. Yazyev, A. J. Austin, R. Cammi, C. Pomelli, J. W. Ochterski, R. L. Martin, K. Morokuma, V. G. Zakrzewski, G. A. Voth, P. Salvador, J. J. Dannenberg, S. Dapprich, A. D. Daniels, Ö. Farkas, J. B. Foresman, J. V. Ortiz, J. Cioslowski, D. J. Fox,

 

Gaussian 09, *Revision A.02*, Gaussian, Inc., Wallingford, CT, USA 2009.
[21] A. D. Becke, *J. Chem. Phys.* **1993**, *98*, 5648.
[22] W. J. Hehre, R. Ditchfield, J. A. Pople, *J. Chem. Phys.* **1972**, *56*, 2257.
[23] E. F. Valeev, V. Coropceanu, D. A. da Silva Filho, S. Salman, J.-L. Bredas, *J. Am. Chem. Soc.* **2006**, *128*, 9882.
[24] D. G. Fedorov, K. Kitaura, *J. Comput. Chem.* **2007**, *28*, 222.
[25] M. W. Schmidt, K. K. Baldridge, J. A. Boatz, S. T. Elbert, M. S. Gordon, J. H. Jensen, S. Koseki, N. Matsunaga, K. A. Nguyen, S. Su, T. L. Windus, M. Dupuis, J. A. Montgomery Jr., *J. Comput. Chem.* **1993**, *14*, 1347.
[26] R. A. Kendall, T. H. Dunning Jr., R. J. Harrison, *J. Chem. Phys.* **1992**, *96*, 6796.